CSIAM Trans. Appl. Math.
doi: 10.4208/csiam-am.SO-2025-0069

Vol. **7**, No. 3, pp. 617-630
May 2026

2D High-Order Cage-Based Deformation by Polygonal Surface Patches

Zeqi Ge[1], Kaikai Qin[1,*], Chongyang Deng[1] and Li-Yong Shen[2]

[1] *School of Science, Hangzhou Dianzi University, Hangzhou 310018, P.R. China.*
[2] *School of Mathematical Sciences, University of Chinese Academy of Sciences, Beijing 100049, P.R. China.*

Received 30 June 2025; Accepted 15 October 2025

Abstract. This paper presents a novel method for 2D high-order cage-based deformation using polygonal surface patches, providing a unified framework that supports various types of polygonal patches. The proposed deformation process comprises two main components: the contribution from the cage corner points and the influence of the middle control points along each boundary curve. First, a coarse deformation is reconstructed using generalized barycentric coordinates derived from the deformed cage corners. Then, displacement curves defined by the middle control points on each cage edge are employed to refine the deformation, precisely relocating the transition points to their final positions. Extensive experimental results demonstrate that our method produces high-quality results across diverse 2D deformation scenarios.

AMS subject classifications: 65D18, 68U05

Key words: Cage-based modeling, 2D shape deformation, polygonal surface patches, generalized barycentric coordinates.

1 Introduction

Cage-based deformation (CBD) [8] has emerged as a widely adopted and effective technique in geometric modeling and computer graphics, providing intuitive shape manipulation through coarse control structures [17]. The method utilizes a simple control mesh (cage) that encapsulates the target object, with deformation governed by generalized barycentric coordinates (GBCs) [2] to establish a mapping between cage vertices and interior points. Despite its effectiveness in various applications, traditional CBD method exhibits two notable limitations due to its linear boundary interpolation: first,

*Corresponding author. *Email addresses:* ge.zeqi@hdu.edu.cn (Z. Ge), qin-kaikai@hdu.edu.cn (K. Qin), dcy@hdu.edu.cn (C. Deng), lyshen@ucas.ac.cn (L. Shen)

the requirement for cage refinement and subsequent GBCs recomputation when additional degrees of freedom are needed [4]; second, the inherent constraint of maintaining piecewise-linear boundary representations [6, 16].

As an extension of traditional CBD, high-order CBD introduces the ability to represent curved cage boundaries, thereby greatly expanding the expressiveness of deformation techniques. Through degree elevation, linear edges of the cage can be transformed into higher-degree Bézier or spline curves by inserting middle control points. This process provides additional degrees of freedom along each boundary segment, allowing for more refined control over shape transformations. By enabling curved cage boundaries, high-order formulations significantly enhance the visual quality of the deformation process, addressing key limitations of linear models in both flexibility and shape fidelity [10]. However, existing high-order CBD methods typically require the surface patches used for deformation to satisfy the property of generalized barycentric reproduction (see Section 4), which limits the adoption of alternative patch types that may offer superior geometric or visual properties.

In this work, we introduce a novel framework for 2D high-order CBD that leverages a broad class of parametric polygonal surface patches. Unlike traditional approaches that are often limited to specific patch types, our method offers a generalized and unified formulation capable of incorporating various polygonal patch representations within a high-order deformation pipeline. For surface patches that inherently support direct deformation, our method yields results equivalent to conventional methods. More importantly, it enables the use of a wider variety of polygonal surface patches that would otherwise be unsuitable for direct deformation, potentially yielding superior results and expanding the applicability of high-order CBD.

The remainder of this paper is organized as follows. Section 2 provides a review of related work on high-order CBD. Section 3 introduces three curve deformation approaches, which are subsequently extended and analyzed for high-order CBD in Section 4. Section 5 presents experimental results and comparisons on various surface patches. Section 6 discusses the limitations of the proposed method. Finally, the paper concludes with a summary of the key contributions.

2 Related work

For high-order CBD through cage coordinates, Li *et al.* [10] first introduced the concept of curved cage boundaries and proposed the cubic mean-value coordinates (MVC). This method transforms linear cages into curved ones by replacing straight edges with cubic Bézier curves, thereby increasing the expressiveness of the deformation. However, as an extension of the classical MVC [3], cubic MVC inherits several inherent limitations. In particular, when applied to non-convex cages, it may generate negative weights, which can lead to visually undesirable artifacts during deformation.

In 2023, Michel and Thiery [14] proposed polynomial Green coordinates (PGC), which extends Green coordinates [12] to support cages with polynomial boundaries. However,

since conformality and interpolation are inherently conflicting properties, the resulting deformations may not adhere tightly to the target boundary. Furthermore, the method requires users to manually define all boundary curves, which reduces usability, and the involved mathematical computations become increasingly complex as the polynomial degree increases.

In 2024, Lin and Chen [11] introduced the polynomial Cauchy coordinates, which generalized Cauchy coordinates [22] to handle Bézier boundaries, enabling both polygon-to-curved and curved-to-curved deformations by leveraging an inverse mapping from an intermediate polygonal domain. While the approach supports flexible and general-purpose deformations, its reliance on inverse mapping introduces numerical instability. A particularly critical drawback is the potential for boundary self-intersections, which can significantly compromise the geometric validity of the resulting shape.

For high-order CBD through polygonal surface patches, Smith and Schaefer [16] proposed a selective degree elevation algorithm based on S-patches [13] in 2015. By applying degree elevation only to selected edges, the method effectively limits the number of control points while transforming linear boundaries into Bézier curve boundaries. However, since the deformation relies solely on the newly inserted control points and lacks global consistency constraints, it often results in unintended distortions.

In 2024, Qin *et al.* [15] proposed a CBD method using C^0 generalized Coons patches (C^0 GC patches). By applying Bézier degree elevation to raise the order of linear cage boundaries, the method obtains additional middle control points, which can then be manipulated to achieve flexible boundary deformation. It also supports the use of arbitrary free-form curves, such as B-splines, to represent cage boundaries.

Over the past few decades, a variety of multi-sided parametric surface patches have been proposed for hole-filling in surface modelling [21]. However, these existing approaches cannot be directly applied to cage-based deformation. Motivated by this limitation, we aim to develop a high-order CBD method that supports various types of polygonal surface patches, enhancing both flexibility and robustness in 2D shape modeling.

3 Curve deformation

To lay the foundation for high-order CBD, we first examine the case of curve deformation in 2D. In the following high-order CBD framework, the original cages are assumed to have linear boundaries, whereas the deformed cages may possess higher-order boundaries. Accordingly, we describe the process by considering an original curve represented as a linear Bézier curve and a deformed curve represented as a d-degree Bézier curve.

Assume that the original curve is defined as

$$\boldsymbol{C}_i(t) = B_0^1(t)\,\boldsymbol{V}_i + B_1^1(t)\,\boldsymbol{V}_{i+1}, \tag{3.1}$$

where $B_0^1(t)$ and $B_1^1(t)$ denote the Bernstein basis functions of degree 1, and $\boldsymbol{V}_i$ and $\boldsymbol{V}_{i+1}$ are their corresponding control points. By applying the degree elevation formula, the

curve can be represented as a Bézier curve of degree d, which introduces $d-1$ middle control points, denoted as $\boldsymbol{P}_1,\boldsymbol{P}_2,\ldots,\boldsymbol{P}_{d-1}$.

The deformation of the Bézier curve is achieved by adjusting these control points. Specifically, the deformed first and last control points are denoted by $\boldsymbol{V}_i'$ and $\boldsymbol{V}_{i+1}'$, while the deformed middle control points are denoted by $\boldsymbol{P}_1',\boldsymbol{P}_2',\ldots,\boldsymbol{P}_{d-1}'$. Our objective is to determine the deformed curve $\boldsymbol{C}_i'(t)$ given these deformed control points.

To the best of our knowledge, existing strategies can be broadly categorized into three main classes [18, 20]. While these approaches are mathematically equivalent in the deformation of a Bézier curve, their implications diverge considerably when extended to high-order CBD. As illustrated in Fig. 1, the process is exemplified for the case where the deformed curve has degree $d=3$.

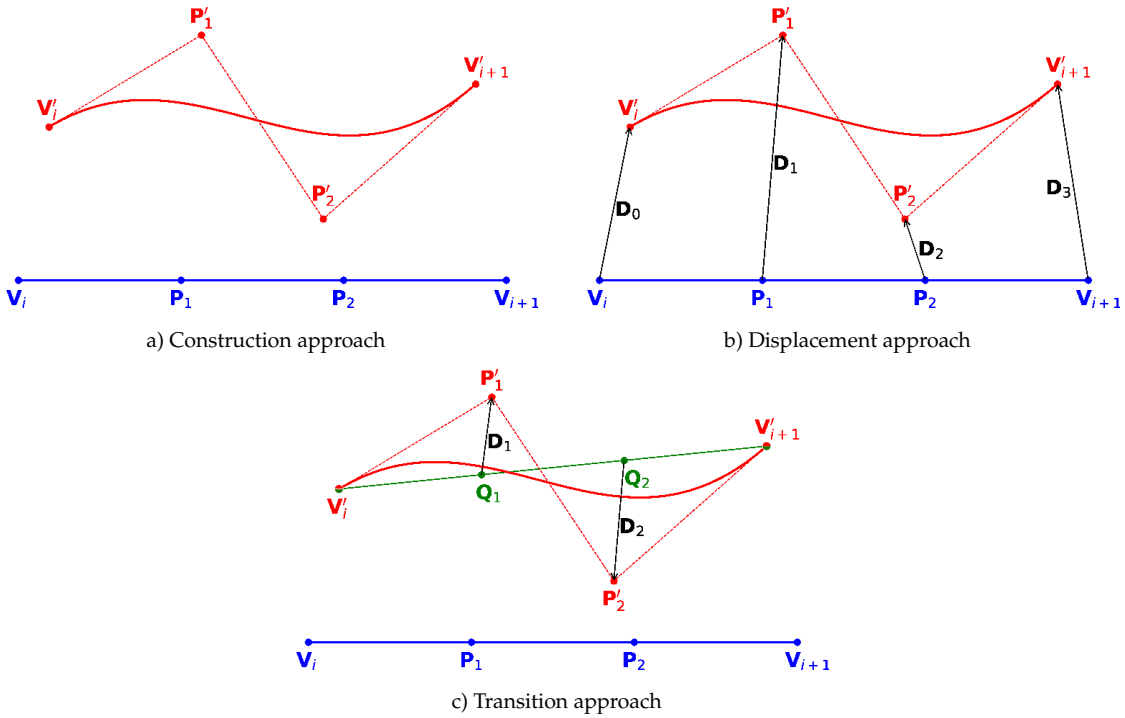

a) Construction approach

b) Displacement approach

c) Transition approach

Figure 1: Three representative approaches to Bézier curve deformation with curves and control polygons shown in blue (original), red (deformed), and green (transitional).

3.1 Construction approach

Given the control points of a Bézier curve, the most straightforward approach to evaluation is through its formulation. The deformed curve can be expressed as

$$\boldsymbol{C}_i'(t)=B_0^d(t)\,\boldsymbol{V}_0'+\sum_{k=1}^{d-1}B_k^d(t)\,\boldsymbol{P}_k'+B_d^d(t)\,\boldsymbol{V}_1', \tag{3.2}$$

where $B_k^d(t)$ denotes the Bernstein basis function of degree d.

3.2 Displacement approach

An alternative approach is to represent the deformation as a displacement from the original curve. Specifically, the displacement vectors associated with the first and last control points are $\boldsymbol{D}_0 = \boldsymbol{V}_i' - \boldsymbol{V}_i$ and $\boldsymbol{D}_d = \boldsymbol{V}_{i+1}' - \boldsymbol{V}_{i+1}$, while those corresponding to the middle control points are $\boldsymbol{D}_k = \boldsymbol{P}_k' - \boldsymbol{P}_k$ for $k = 1,2,\ldots,d-1$. Accordingly, the displacement curve is defined as

$$\boldsymbol{C}_D(t) = \sum_{k=0}^{d} B_k^d(t)\,\boldsymbol{D}_k. \tag{3.3}$$

In this case, the deformed curve is expressed as the sum of the original curve and the displacement curve

$$\boldsymbol{C}_i'(t) = \boldsymbol{C}_i(t) + \boldsymbol{C}_D(t). \tag{3.4}$$

3.3 Transition approach

Another approach is to employ a transitional curve as the reference, rather than the original curve. Specifically, a linear Bézier curve is first constructed from the deformed endpoints $\boldsymbol{V}_i'$ and $\boldsymbol{V}_{i+1}'$

$$\boldsymbol{C}_T(t) = B_0^1(t)\,\boldsymbol{V}_i' + B_1^1(t)\,\boldsymbol{V}_{i+1}', \tag{3.5}$$

which we refer to as the transitional curve. This curve is then elevated to degree d, thereby introducing $d-1$ middle control points, denoted as $\boldsymbol{Q}_1, \boldsymbol{Q}_2, \ldots, \boldsymbol{Q}_{d-1}$.

Analogous to Section 3.2, a displacement curve $\boldsymbol{C}_D(t)$ is introduced to capture the deviation of the deformed curve from the transitional curve. Since the endpoints of the transitional curve already coincide with those of the deformed curve, the displacement vectors at the first and last control points vanish, i.e. $\boldsymbol{D}_0 = \boldsymbol{0}$ and $\boldsymbol{D}_d = \boldsymbol{0}$. Consequently, the deformed curve can be expressed as the sum of the transitional curve and the displacement curve

$$\boldsymbol{C}_i'(t) = \boldsymbol{C}_T(t) + \boldsymbol{C}_D(t). \tag{3.6}$$

4 High-order cage-based deformation

Let the original cage be a closed polygon with n vertices $\boldsymbol{V}_1, \boldsymbol{V}_2, \ldots, \boldsymbol{V}_n$. Each boundary curve is represented by a linear Bézier curve $\boldsymbol{C}_i$ with endpoints $\boldsymbol{V}_i$ and $\boldsymbol{V}_{i+1}$. We denote by Ω the original cage space, i.e. the cage together with its enclosed interior region. After deformation, the corner vertices of the cage are relocated to $\boldsymbol{V}_1', \boldsymbol{V}_2', \ldots, \boldsymbol{V}_n'$, and each deformed boundary curve $\boldsymbol{C}_i'$ is defined with endpoints $\boldsymbol{V}_i'$ and $\boldsymbol{V}_{i+1}'$. Correspondingly, the deformed cage space is denoted by Ω'.

When a selected patch is employed for 2D deformation, its domain polygon is Ω. For any point $\boldsymbol{x} \in \Omega$, its GBCs with respect to the n cage vertices are written as $(\lambda_1, \lambda_2, \ldots, \lambda_n)$. The patch can be regarded as a mapping $\boldsymbol{S}: \Omega \to \mathbb{R}^2$. In particular, if the patch satisfies the

generalized barycentric reproduction property [15], namely, when its boundary curve is linear, it reduces to the identity mapping

$$\boldsymbol{S}(\boldsymbol{x})=\sum_{i=1}^{n}\lambda_i \boldsymbol{V}_i=\boldsymbol{x}. \tag{4.1}$$

For the deformed patch $\boldsymbol{S}'$, the domain polygon remains Ω, while only the configuration of its boundary curve is modified. In this work, we primarily employ the side-blend patch [9, 21], which does not possess this property, and compare it against patches that do, including the C^0 GC patches [15], the generalized Bézier (GB) patches [18, 19], and the selective degree elevation for S-patches [16].

It is widely recognized that the construction of most multi-sided parametric surface patches is based on local parameterizations, which transform a quadrilateral domain defined by a specific side or corner into the corresponding multi-sided domain [21]. In this work, we adopt the "side" and "distance" parameters from GBCs. Accordingly, for the i-th edge of Ω, we define its side parameter and distance parameter as follows:

$$s_i(\boldsymbol{x})=\frac{\lambda_{i+1}}{\lambda_i+\lambda_{i+1}},\quad d_i(\boldsymbol{x})=1-\lambda_i-\lambda_{i+1}. \tag{4.2}$$

Fig. 2 illustrates the isolines of s_i and d_i in both convex and concave polygons. The s_i-isolines sweep across the domain from the $(i-1)$-th side to the $(i+1)$-th side, while the d_i-isolines emanate from the i-th side and extend toward the opposite sides of the domain. Together, these two families of parameter lines establish a structured coordinate system for multi-sided surface patches.

The high-order CBD deformation process consists of two stages.

1. **Binding**: Reproduces the entire cage space using GBCs

$$\boldsymbol{x}=\sum_{i=1}^{n}\lambda_i \boldsymbol{V}_i. \tag{4.3}$$

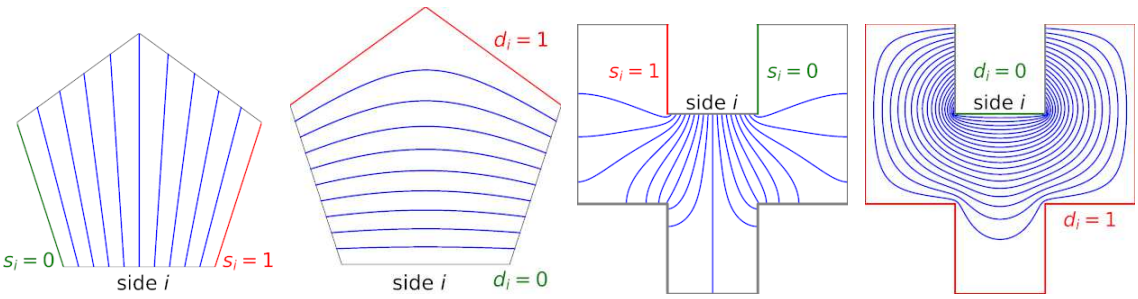

a) s_i in convex polygon b) d_i in convex polygon c) s_i in concave polygon d) d_i in concave polygon

Figure 2: Isolines of the s_i and d_i in both convex and concave polygons.

2. **Deformation**: Deforms the cage space by adjusting the boundary curves

$$\boldsymbol{C}_i(s_i) \to \boldsymbol{C}_i'(s_i). \tag{4.4}$$

The goal is to derive Ω', namely the deformed position $\boldsymbol{x}'$ corresponding to each $\boldsymbol{x}$. As in Section 3, three approaches can be employed to achieve this deformation.

4.1 Construction approach

The most straightforward approach is to directly apply the selected patch formula to the deformed boundary curves. Therefore, the deformed position can be computed as

$$\boldsymbol{x}' = \boldsymbol{S}'(\boldsymbol{x}). \tag{4.5}$$

However, its applicability is restricted to surface patches that satisfy the generalized barycentric reproduction property. In the absence of this property, the resulting deformation may becomes invalid.

4.2 Displacement approach

An alternative approach is to represent the deformation using some displacement curves. First, reconstruct the original position using GBCs

$$\boldsymbol{x} = \sum_{i=1}^{n} \lambda_i \boldsymbol{V}_i. \tag{4.6}$$

Then, for the i-th boundary curve, define a displacement curve to represent its deformation

$$\boldsymbol{C}_{i,D}(s_i) = \sum_{k=0}^{d} B_k^d(s_i)\, \boldsymbol{D}_k. \tag{4.7}$$

Finally, by adding the displacement curves of all boundary curves to the original position, we obtain the deformed position

$$\boldsymbol{x}' = \boldsymbol{x} + \sum_{i=1}^{n} W_i \boldsymbol{C}_{i,D}(s_i), \tag{4.8}$$

where W_i denotes the blend function associated with the i-th side of the selected patch.

Table 1 presents the blend functions for the C^0 GC patch and the side-blend patch, and Fig. 3 further illustrates the contour maps of W_i, providing a comparison between the two patches in both convex and concave polygonal domains. For the C^0 GC patch, it is constructed based on the Boolean sum formulation, where side interpolants are combined with side blends, and correction surfaces are coupled with corner blends. Consequently, the corresponding side blend function W_i is influenced by three adjacent sides. Specifically, the side blend function is nonzero only across three sides: It takes the value 1 on

Table 1: Blend functions of various patches, with $\alpha_i = d_{i-1}/(d_{i-1}+d_i)$ and $\beta_i = d_{i+1}/(d_{i+1}+d_i)$.

Patch	Blend function
C^0 GC	$W_i = \lambda_i + \lambda_{i+1}$
Side-blend	$W_i = \dfrac{(\lambda_i+\lambda_{i+1})\alpha_i\beta_i}{\sum_{k=1}^{n}(\lambda_k+\lambda_{k+1})\alpha_k\beta_k}$

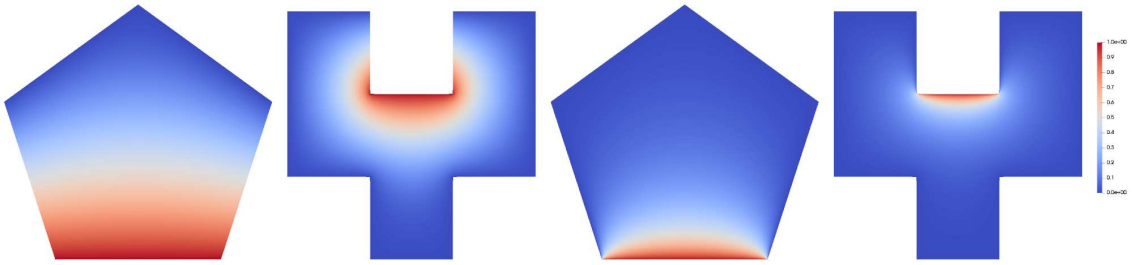

Figure 3: Contour plots of W_i for convex and concave polygons: C^0 GC patch (left two) and side-blend patch (right two).

side i, gradually decreases on sides $i-1$ and $i+1$, and vanishes at the respective adjacent corners. In contrast, the side-blend patch is formed as a convex combination of the interpolants defined along the edges. Its side blend function is localized: It takes the value 1 exclusively on the i-th side and remains zero on all other sides.

4.3 Transition approach

Another approach is to use a transitional position as the base. First, reconstruct the transitional position using GBCs

$$\boldsymbol{x}'_T = \sum_{i=1}^{n} \lambda_i \boldsymbol{V}'_i. \tag{4.9}$$

Then, for the i-th boundary curve, define a displacement curve to represent its deformation. Unlike the previous displacement method, the endpoints here remain fixed, so their displacement vectors are zero. Finally, by adding the displacement curves of all boundary curve to the transitional position, we obtain the deformed position

$$\boldsymbol{x}' = \boldsymbol{x}'_T + \sum_{i=1}^{n} W_i \boldsymbol{C}_{i,D}(s_i). \tag{4.10}$$

For the three approaches, the C^0 GC patch, GB patch, and S-patch can all adopt the construction approach, whereas this approach is not applicable to the side-blend patch. With respect to the displacement and transition approaches, for the C^0 GC patch and GB patch, the transition approach produces results identical to those obtained with the construction approach, whereas the displacement approach does not. In contrast, for the

side-blend patch, the transition approach yields superior results compared to the displacement approach. A visual comparison of these outcomes is provided in Fig. 4.

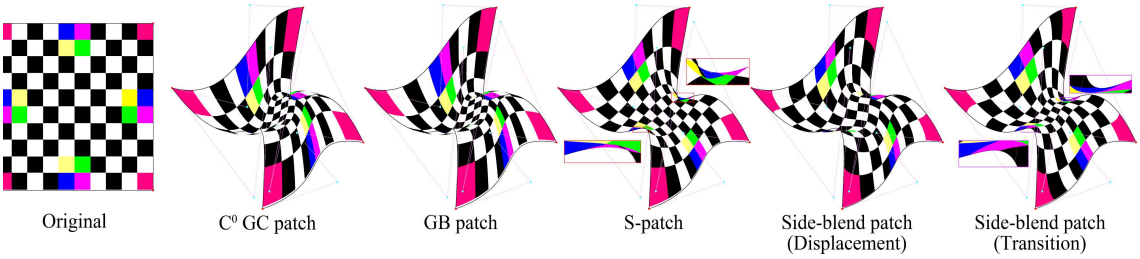

Figure 4: Deformation results for a square-shaped. All cases employ the same cubic cage and are evaluated on four types of surface patches: the C^0 generalized Coons patch, the generalized Bézier patch, the selective degree elevation for S-patch, and the side-blend patch. For the side-blend patch, results from both the displacement and transition approaches are presented. Wachspress coordinates [6] are used to evaluate all patches.

5 Results

In this section, we compare several results to demonstrate the effectiveness of our method.

As illustrated in Fig. 4, the C^0 GC patch and the GB patch exhibit noticeable distortion, while the S-patch introduces visible artifacts (in the red frames). For the side-blend patch, the displacement approach results in significant visual distortion. In contrast, the transition approach yields comparatively better results (in the purple frames).

Moreover, we analyze the distortion of the mapping from the original cage space Ω to the deformed cage space Ω'. Fig. 5(a) shows the area distortion, evaluated by the determinant $\det(J_f)$ of the Jacobian J_f for each triangular face f. Here, $\det(J_f)=1$ indicates area preservation, $\det(J_f)>0$ with values $\neq 1$ indicates local scaling (expansion or contraction), and $\det(J_f)<0$ indicates fold-overs. Fig. 5(b) shows the angle distortion, measured by the most isometric parametrizations (MIPS) energy [1, 5] $\mathrm{trace}(J_f^\top J_f)/\det(J_f)$. The minimum value of 2 is attained precisely when J_f is a similarity transformation (angle-preserving), while larger values indicate higher angular distortion. For visualization purposes, flipped triangles are assigned a MIPS energy of -1 to clearly indicate fold-overs in the plots.

As illustrated in Fig. 5, for the C^0 GC patch, GB patch, S-patch, and side-blend patch with displacement approach, fold-overs occur on both sides of the domain (pink regions). Furthermore, the Jacobian determinant plot reveals that the area distortion is particularly severe near the lower-left and upper-right corners. Consistently, the MIPS energy visualization highlights higher energy values along both sides of the domain (cyan regions). By contrast, the side-blend patch with transition approach produces relatively better result compared to the other methods.

In Fig. 6, both the C^0 GC patch and the GB patch exhibit unintuitive behavior: When the upper-right corner is displaced, the character's head bends leftward, causing the facial expression to shift in the opposite direction. By contrast, the S-patch and the side-

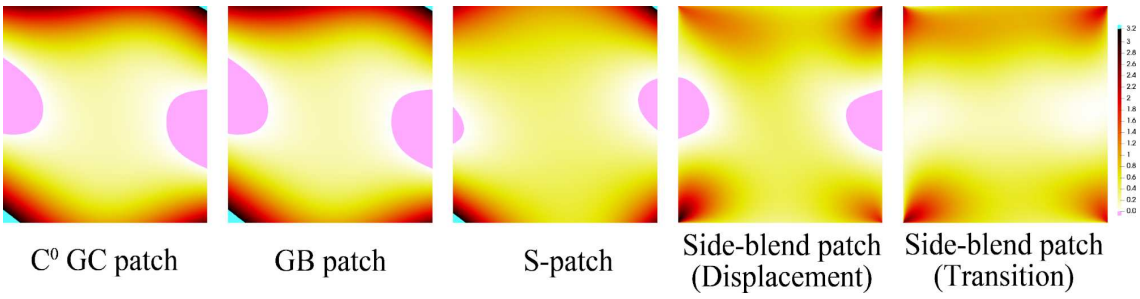

a) Area distortion: Jacobian determinant

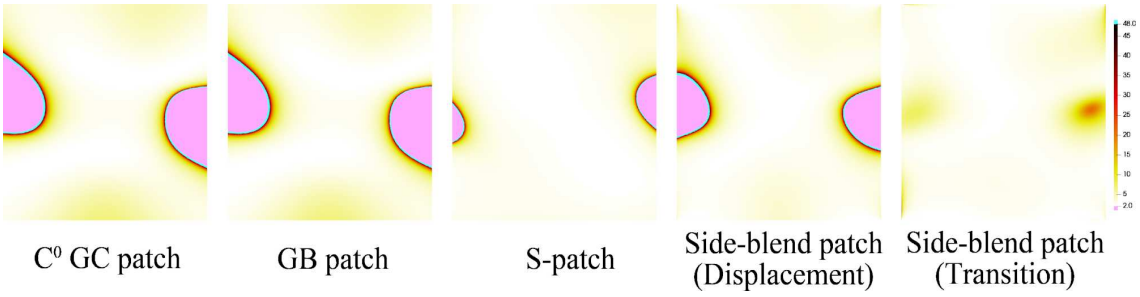

b) Angle distortion: MIPS energy

Figure 5: Area and angular distortion of the deformation shown in Fig. 4. Top row: Jacobian determinant visualizing area distortion. Bottom row: MIPS energy indicating angular distortion.

blend patch produce more natural deformations. The differences are further highlighted by the texture on the character's right arm: While the C^0 GC patch and the GB patch induce a leftward drift, the S-patch generates a slight rightward shift, and the side-blend patch maintains an almost vertical alignment.

As shown in Fig. 7, although the S-patch produces slightly inferior deformation results, all methods are still able to complete the model deformation. Nevertheless, across the entire cage-space, the C^0 GC patch, GB patch, and S-patch still produce fold-overs in certain regions (red frames). In contrast, the side-blend patch achieves deformations without visible artifact (purple frame).

Although the side-blend patch achieves favorable deformation results, the transition approach cannot guarantee fold-over free mappings. As shown in Fig. 8, all other patches exhibit noticeable fold-overs on the model, while the side-blend patch performs well in these regions. In the distortion visualization of Fig. 9, the side-blend patch also presents some fold-overs (pink regions); however, these are confined to smaller areas, thereby demonstrating its superior performance compared to the other patches.

Finally, Fig. 10 provides a gallery of deformation results obtained with the side-blend patch under the transition approach, demonstrating that its performance is superior to the other three patches discussed in this paper.

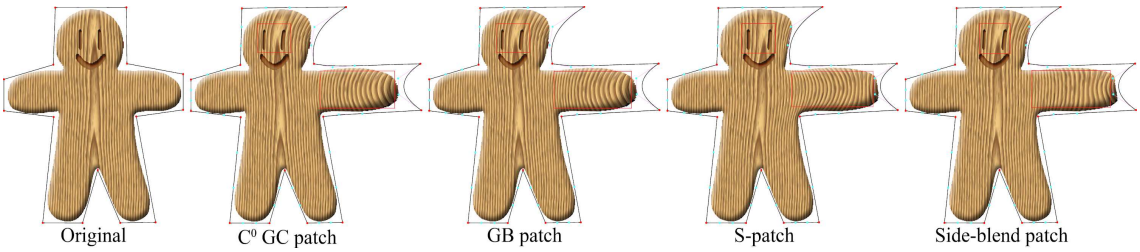

Figure 6: Deformation results of the gingerbread-man model. From left to right: the original cage and object, deformed results obtained using the C^0 GC patch, GB patch, selective degree elevation for S-patch, and side-blend patch with the transition approach. Harmonic coordinates [7] are used to evaluate all patches.

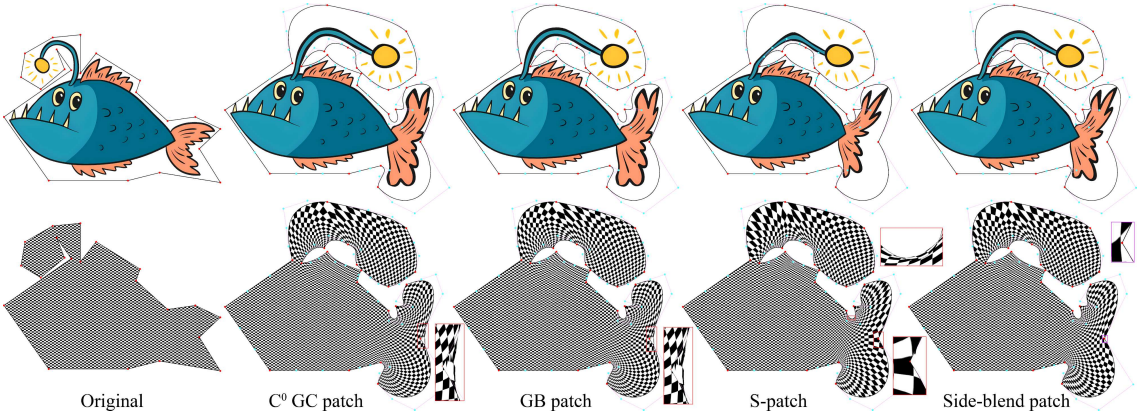

Figure 7: Deformation results of the fish model. From left to right: the original cage and object, deformed results obtained using the C^0 GC patch, GB patch, selective degree elevation for S-patch, and side-blend patch with the transition approach. Harmonic coordinates [7] are used to evaluate all patches.

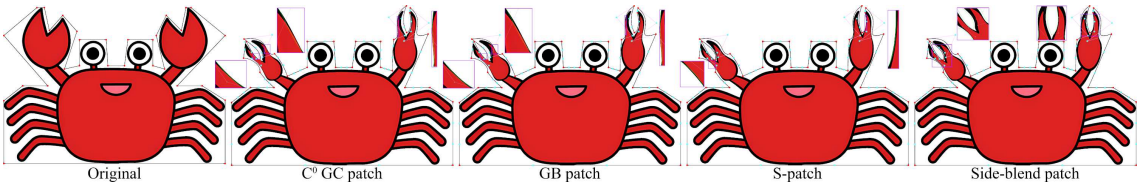

Figure 8: Deformation results of the crab model. From left to right: the original cage and object, deformed results obtained using the C^0 GC patch, GB patch, selective degree elevation for S-patch, and side-blend patch with the transition approach. Harmonic coordinates [7] are used to evaluate all patches.

6 Limitations and future work

Although our method demonstrates effective 2D CBDs using various polygonal surface patches, several limitations remain, offering promising directions for future research.

First, the current approach does not provide a theoretical guarantee of foldover-free deformation. This is primarily because the deformation is computed via explicit barycentric interpolation combined with displacement correction, without incorporating global

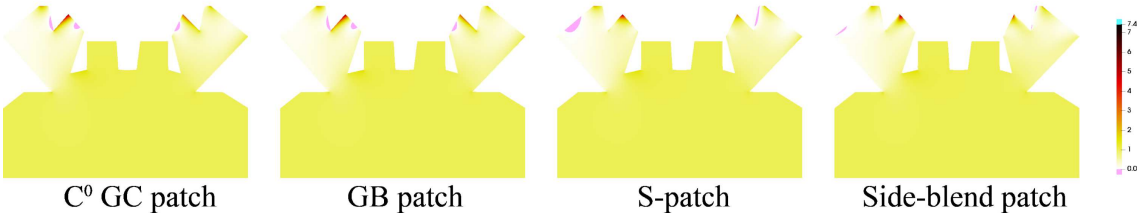

a) Area distortion: Jacobian determinant

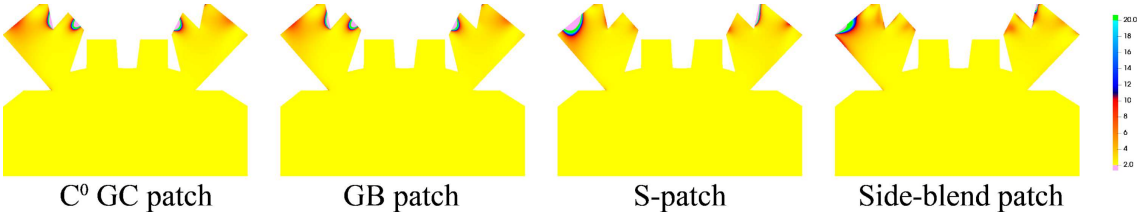

b) Angle distortion: MIPS energy

Figure 9: Area and angular distortion of the deformation shown in Fig. 8. Top row: Jacobian determinant visualizing area distortion. Bottom row: MIPS energy indicating angular distortion.

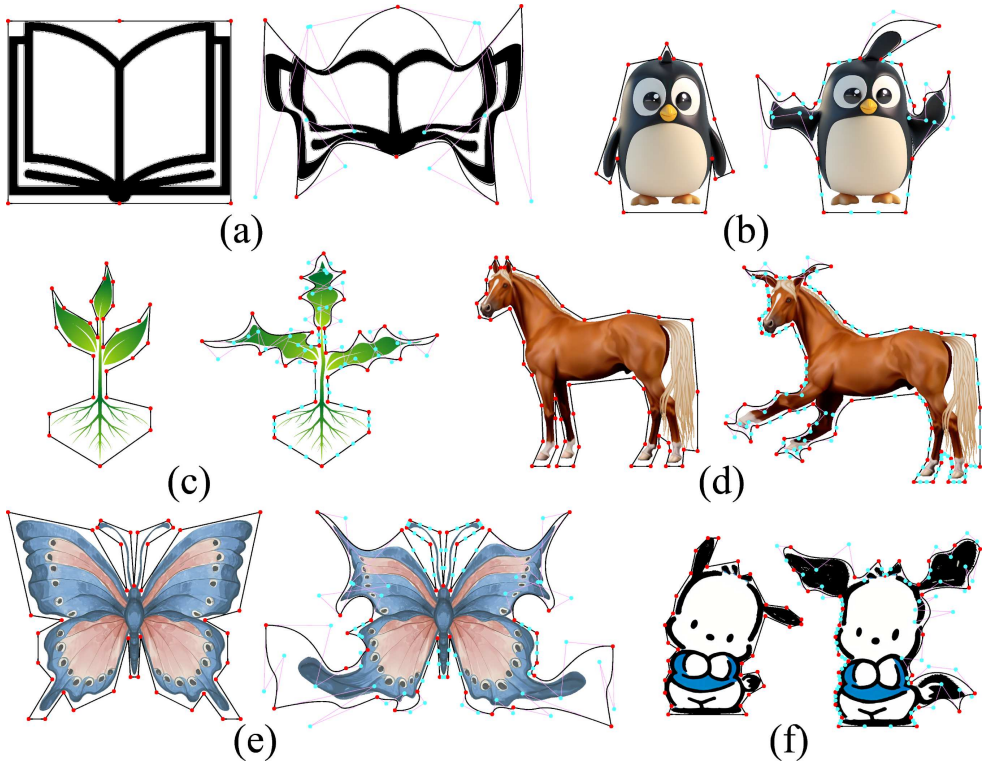

Figure 10: Gallery of deformation results using the side-blend patch with transition approach. (a) Book - page warping on both sides; (b) Penguin - unrealistic arm articulation during dance motion; (c) Plant - leaf curvature artifacts; (d) Horse - ear deformation and unnatural leg elevation; (e) Butterfly - wing bending distortions; (f) Pochacco - exaggerated ear and tail reaction.

injectivity constraints or optimization-based safeguards. While experimental results show that our method produces high-quality deformations even for surface patches lacking the property of generalized barycentric reproduction, establishing theoretical guarantees remains an open challenge for future work.

Second, the current approach relies exclusively on generalized barycentric coordinates computed with respect to a linear cage. While this provides good deformation behavior, it limits the expressiveness of the deformation space. An interesting direction for future research is to investigate the integration of higher-order cage coordinates into our framework to further enhance deformation quality and flexibility.

Third, our current method is designed and evaluated only in the 2D setting. Extending the proposed high-order deformation strategies to 3D remains an open and challenging problem. Future work will investigate whether a unified framework can be developed for 3D surface or volumetric deformation, leveraging analogous principles of polygonal patches and generalized coordinates in higher dimensions.

Conclusion

We have presented a novel deformation method that unifies various types of polygonal surface patches for 2D high-order cage-based deformation. Our framework allows different patch types to be used interchangeably within a single, coherent approach, thereby enhancing flexibility and expressiveness in shape modeling. The experimental results indicate that even surface patches without the generalized barycentric reproduction property (e.g. side-blend patches) can yield superior outcomes under this approach compared to those that possess the property. Moreover, based on extensive experimental results and quantitative observations, we find that the outcomes and metrics of the C^0 GC patch and the linear GB patch are identical, indicating that they are fully equivalent. By providing a unified and consistent framework, our work broadens the applicability of polygonal surface patches in computer graphics and geometric modeling, and offers a robust, versatile foundation for high-order 2D deformation tasks.

Acknowledgments

The authors gratefully acknowledge all the reviewers for their careful evaluation and insightful comments. We also wish to express our sincere appreciation to the conference organizers and the journal editorial office for their continuous support and assistance throughout the review and publication process. Special appreciation is extended to Prof. Kai Hormann of Università della Svizzera Italiana (USI) for his invaluable guidance and thoughtful advice on the revisions of this work during the authors' stay at USI.

This work was supported by the National Natural Science Foundation of China (NSFC) under Project No. 61872121.

References

[1] Q. J. Chang, C. Y. Deng, and K. Hormann, *Maximum likelihood coordinates*, Comput. Graph. Forum, 42(5):e14908, 2023.

[2] M. S. Floater, *Generalized barycentric coordinates and applications*, Acta Numer., 24:161–214, 2015.

[3] M. S. Floater, *Mean value coordinates*, Comput. Aided Geom. Des., 20(1):19–27, 2003.

[4] K. Hormann and M. S. Floater, *Mean value coordinates for arbitrary planar polygons*, ACM Trans. Graph., 25(4):1424–1441, 2006.

[5] K. Hormann and G. Greiner, *MIPS: An efficient global parametrization method*, in: Curve and Surface Design, 153–162, Vanderbilt University Press, 2000.

[6] K. Hormann and N. Sukumar, *Generalized Barycentric Coordinates in Computer Graphics and Computational Mechanics*, CRC Press, 2017.

[7] P. Joshi, M. Meyer, T. DeRose, B. Green, and T. Sanocki, *Harmonic coordinates for character articulation*, ACM Trans. Graph., 26(3):71–es, 2007.

[8] T. Ju, S. Schaefer, and J. Warren, *Mean value coordinates for closed triangular meshes*, ACM Trans. Graph., 24(3):561–566, 2005.

[9] K. Kato, *Generation of n-sided surface patches with holes*, Comput. Aided Des., 23(10):676–683, 1991.

[10] X. Y. Li, T. Ju, and S. M. Hu, *Cubic mean value coordinates*, ACM Trans. Graph., 32(4):126, 2013.

[11] Z. H. Lin and R. J. Chen, *Polynomial Cauchy coordinates for curved cages*, in: SIGGRAPH Asia 2024 Conference Papers, 67, 2024.

[12] Y. Lipman, L. David, and C. Daniel, *Green coordinates*, ACM Trans. Graph., 27(3):78, 2008.

[13] C. T. Loop and T. D. DeRose, *A multisided generalization of Bézier surfaces*, ACM Trans. Graph., 8(3):204–234, 1989.

[14] É. Michel and J. M. Thiery, *Polynomial 2D Green coordinates for polygonal cages*, in: ACM SIGGRAPH 2023 Conference Proceedings, 23, 2023.

[15] K. K. Qin, Y. H. Zhou, C. H. Ying, Y. J. Li, and C. Y. Deng, *C^0 generalized Coons patches for high-order cage-based deformation*, ACM Trans. Graph., 43(6):220, 2024.

[16] J. Smith and S. Schaefer, *Selective degree elevation for multi-sided Bézier patches*, Comput. Graph. Forum, 34(2):609–615, 2015.

[17] D. Ströter, J. M. Thiery, K. Hormann, J. Chen, Q. Chang, S. Besler, J. S. Mueller-Roemer, T. Boubekeur, A. Stork, and D. W. Fellner, *A survey on cage-based deformation of 3D models*, Comput. Graph. Forum, 43(2):e15060, 2024.

[18] T. Várady, P. Salvi, and G. Karikó, *A multi-sided Bézier patch with a simple control structure*, Comput. Graph. Forum, 35(2):307–317, 2016.

[19] T. Várady, P. Salvi, and I. Kovács, *Enhancement of a multi-sided Bézier surface representation*, Comput. Aided Geom. Des., 55:69–83, 2017.

[20] T. Várady, P. Salvi, and M. Vaitkus, *Generalized Bézier and B-spline patches with exact refinement*, in: Proceedings of the Eleventh Hungarian Conference on Computer Graphics and Geometry, 1–5, 2024. `http://3dgeo.iit.bme.hu/papers/multisided/refinement.pdf`

[21] T. Várady, P. Salvi, and M. Vaitkus, *Genuine multi-sided parametric surface patches – A survey*, Comput. Aided Geom. Des., 110:102286, 2024.

[22] O. Weber, M. Ben-Chen, and C. Gotsman, *Complex barycentric coordinates with applications to planar shape deformation*, Comput. Graph. Forum, 28(2):587–597, 2009.